Published in final edited form as:
Sci Transl Med. 2011 March 16; 3(74): 74ra24. doi:10.1126/scitranslmed.3001868.

The *ΔF508* Mutation Causes CFTR Misprocessing and Cystic Fibrosis-Like Disease in Pigs

Lynda S Ostedgaard[1,*], **David K Meyerholz**[2,*], **Jeng-Haur Chen**[1,5,*], **Alejandro A Pezzulo**[1], **Philip H Karp**[1,5], **Tatiana Rokhlina**[1], **Sarah E Ernst**[1], **Robert A Hanfland**[3], **Leah R Reznikov**[1], **Paula S Ludwig**[1], **Mark P Rogan**[1], **Greg J Davis**[1], **Cassie L Dohrn**[2], **Christine Wohlford-Lenane**[4], **Peter J Taft**[1], **Michael V Rector**[1], **Emma Hornick**[1], **Boulos S Nassar**[1], **Melissa Samuel**[6], **Yuping Zhang**[1], **Sandra S Richter**[2], **Aliye Uc**[4], **Joel Shilyansky**[3], **Randall S Prather**[6], **Paul B McCray Jr.**[4], **Joseph Zabner**[1], **Michael J Welsh**[1,5], and **David A Stoltz**[1]

[1] Department of Internal Medicine, Roy J. and Lucille A. Carver College of Medicine, University of Iowa, Iowa City, IA 52242

[2] Department of Pathology, Roy J. and Lucille A. Carver College of Medicine, University of Iowa, Iowa City, IA 52242

[3] Department of Surgery, Roy J. and Lucille A. Carver College of Medicine, University of Iowa, Iowa City, IA 52242

[4] Department of Pediatrics, Roy J. and Lucille A. Carver College of Medicine, University of Iowa, Iowa City, IA 52242

[5] Howard Hughes Medical Institute, Roy J. and Lucille A. Carver College of Medicine, University of Iowa, Iowa City, IA 52242

[6] Division of Animal Sciences, University of Missouri, Columbia, MO 65211

Abstract

Mutations in the gene encoding the cystic fibrosis transmembrane conductance regulator (CFTR) anion channel cause the autosomal recessive disease, cystic fibrosis (CF). The most common mutation is *ΔF508*, which deletes phenylalanine508. *In vitro* studies indicate that CFTR-ΔF508 is misprocessed, though *in vivo* consequences of the mutation are uncertain. To better understand effects of the *ΔF508* mutation, we produced $CFTR^{\Delta F508/\Delta F508}$ pigs. Our biochemical, immunocytochemical and electrophysiological data on CFTR-ΔF508 in newborn pigs paralleled *in vitro* results. They also indicated that $CFTR^{\Delta F508/\Delta F508}$ airway epithelia retain a small residual CFTR conductance; maximal stimulation produced ~6% of wild-type function. Interestingly, cAMP agonists were less potent at stimulating current in $CFTR^{\Delta F508/\Delta F508}$ epithelia, suggesting that quantitative tests of maximal anion current may overestimate transport under physiological conditions. Despite residual CFTR function, four older $CFTR^{\Delta F508/\Delta F508}$ pigs developed lung disease strikingly similar to human CF. These results suggest that this limited CFTR activity is insufficient to prevent lung or gastrointestinal disease in CF pigs. These data also suggest that studies of recombinant CFTR-ΔF508 misprocessing predict *in vivo* behavior, which validates its use in biochemical and drug discovery experiments. These findings help elucidate the molecular pathogenesis of the common CF mutation and will guide strategies for developing new therapeutics.

Address correspondence to: Michael J. Welsh, Howard Hughes Medical Institute, Roy J. and Lucille A. Carver College of Medicine, 500 EMRB, Iowa City, IA 52242, Phone: 319-335-7619, FAX: 319-335-7623, michael-welsh@uiowa.edu or David A. Stoltz, Roy J. and Lucille A. Carver College of Medicine, 440 EMRB, Iowa City IA 52242, Phone: 319-336-1620, FAX: 319-335-7623, david-stoltz@uiowa.edu.
*These authors made equal contributions.

INTRODUCTION

Cystic fibrosis (CF) is a common life-shortening, autosomal recessive disease caused by mutations in the gene encoding the CFTR anion channel (1). CFTR is expressed in epithelia of multiple organs and its loss causes airway, pancreatic, intestinal, liver, and vas deferens disease. The *ΔF508* mutation (also called *F508del*), is the most common CF-causing mutation, accounting for ~70% of CF alleles; most patients carry at least one *ΔF508* allele.

Numerous studies have expressed human CFTR-ΔF508 *in vitro* and found that its biosynthetic processing is disrupted; the mutant protein is retained in the endoplasmic reticulum (ER) and rapidly degraded (2–4). As a result, CFTR-ΔF508 fails to reach the apical membrane. CFTR-ΔF508 can be induced to traffic to the cell surface by reducing the incubation temperature or adding chemicals that facilitate folding, and once at the membrane, it retains channel function, although its lifetime and open state probability are reduced (5–9). These discoveries sparked an effort by academia and industry to therapeutically correct the CFTR-ΔF508 defects (10,11).

However, the conclusion that CFTR-ΔF508 biosynthesis is disrupted has relied largely on studies of recombinant protein (2–4). It has been much more difficult to study the endogenous protein because of limited human tissue availability, the small amount of CFTR in affected epithelia, and changes caused by inflammation and tissue remodeling of advanced CF. Studies of endogenous CFTR have sometimes reached conclusions that contrast strikingly with data from recombinant systems. For example, some reports indicated that CFTR-ΔF508 was processed and localized like wild-type CFTR (12,13). Other reports suggested that CFTR-ΔF508 reached the apical membrane, but in reduced amounts(14,15). Still other reports indicated that CFTR-ΔF508 was either not detectable or did not reach the apical membrane (16–18). In addition, although most studies did not detect Cl^- channel function in freshly excised *ΔF508/ΔF508* airway epithelial cells, others have identified residual Cl^- transport (19,20). The reasons for these varying conclusions are uncertain, but obtaining the cells and tissues from airways with infection, inflammation and remodeling might have affected results (14).

Efforts to understand abnormalities produced by the *ΔF508* mutation have been hindered by lack of an animal model that expresses CFTR-ΔF508 and manifests a typical CF phenotype. This limitation has also hindered attempts to target CFTR-ΔF508 therapeutically, and it has impeded efforts to understand pathogenesis. Unfortunately, mice with *CFTR* gene mutations, including *ΔF508*, do not develop airway disease typical of human CF (21). The newly developed $CFTR^{-/-}$ pig and ferret models may offer an opportunity to better understand disease pathogenesis (22,23). At birth, $CFTR^{-/-}$ pigs exhibit a phenotype like that in patients with CF, including pancreatic destruction, meconium ileus, early focal biliary cirrhosis, and microgallbladder (22,24). Like lungs from newborn humans with CF, lungs from newborn $CFTR^{-/-}$ pigs show no evidence of inflammation, but with time they spontaneously develop lung disease with the characteristic features of CF including inflammation, infection, mucus accumulation, tissue remodeling, and airway obstruction (25).

Encouraged by the phenotype of $CFTR^{-/-}$ pigs, we set out to generate $CFTR^{\Delta F508/\Delta F508}$ pigs. Our initial goal was to answer three key questions. First, would $CFTR^{\Delta F508/\Delta F508}$ pigs have the same or a different clinical phenotype as pigs with a complete lack of CFTR? Residual CFTR activity might ameliorate disease severity compared to $CFTR^{-/-}$ pigs, or alternatively, the presence of the mutant protein might worsen disease manifestations. Second, would porcine CFTR-ΔF508 be misprocessed *in vivo*? In earlier work, we found

that although porcine CFTR-ΔF508 was largely misprocessed *in vitro*, a small fraction was correctly processed and delivered to the epithelial apical membrane where it generated some Cl^- conductance (26). We wondered if this would also occur *in vivo*. The results would have important implications for studies of mechanism and for strategies to therapeutically target CFTR-ΔF508. Third, if CFTR-ΔF508 was partially processed in *CFTR*$^{\Delta F508/\Delta F508}$ pigs and retained some anion transport function, it would provide us with an opportunity to begin to answer an important question for therapeutic strategies, i.e., how much airway epithelial anion channel activity is sufficient to prevent CF lung disease?

RESULTS

We generated *CFTR*$^{\Delta F508/\Delta F508}$ pigs

We previously generated male *CFTR*$^{\Delta F508/+}$ pigs using somatic cell nuclear transfer and embryo transfer (27). The nucleotide sequence …*ATC-TTT-GGT*…, which encodes …I507-F508-G509…, is identical in exon 10 of porcine and human *CFTR*. To reproduce the human mutation, we deleted *C-TT* (i.e., the*ΔF508* allele) to generate …*ATT-GGT*.., which encodes …I507-G509…. In addition, the intron downstream of exon 10 contains a Neo^R cassette.

We crossed *CFTR*$^{\Delta F508/+}$ males, which had a normal clinical phenotype, to wild-type females to generate *CFTR*$^{\Delta F508/+}$ female pigs. We then crossed *CFTR*$^{\Delta F508/+}$ males and females to generate *CFTR*$^{\Delta F508/\Delta F508}$ pigs. The ratio of *CFTR*$^{\Delta F508/\Delta F508}$:*CFTR*$^{\Delta F508/+}$:*CFTR*$^{+/+}$ pigs, 82:129:63, did not differ statistically (chi-squared test) from the predicted Mendelian ratio of 1:2:1.

Newborn *CFTR*$^{\Delta F508/\Delta F508}$ pigs have pathology like that of *CFTR*$^{-/-}$ pigs

Like *CFTR*$^{-/-}$ and *CFTR*$^{\Delta F508/-}$ piglets (24,25), *CFTR*$^{\Delta F508/\Delta F508}$ pigs had meconium ileus with 100% penetrance. The site of obstruction varied, but was generally near the ileocecal junction (Fig. 1A). Distal to the obstruction, the intestine was of small caliber and variably filled with mucocellular debris (Fig. 1B). We did not discern differences between the intestinal pathology or meconium ileus of *CFTR*$^{\Delta F508/\Delta F508}$ and *CFTR*$^{-/-}$ pigs.

In the pancreas, lobular parenchyma was decreased in *CFTR*$^{\Delta F508/\Delta F508}$ pigs (Fig. 1C). Pancreatic acini and ducts were often dilated by zymogen concretions with scattered neutrophils, macrophages and mucus, like that found in newborn *CFTR*$^{-/-}$ pigs (24). *CFTR*$^{\Delta F508/\Delta F508}$ pancreata had reduced parenchyma compared to *CFTR*$^{+/+}$, but the destruction was slightly less severe than in *CFTR*$^{-/-}$ (Fig. 1D).

The *CFTR*$^{\Delta F508/\Delta F508}$ liver had focal portal areas expanded by bile duct proliferation, inflammation, and/or increased connective tissue, changes characteristic of early focal biliary cirrhosis (Fig. 1E). The frequency and severity of changes were similar to those we observed in *CFTR*$^{-/-}$ pigs (24). Likewise, the microgallbladder and mucinous changes in gallbladder epithelia observed in *CFTR*$^{-/-}$ pigs were ubiquitous in *CFTR*$^{\Delta F508/\Delta F508}$ animals (Fig. 1F).

Airway epithelia of newborn *CFTR*$^{\Delta F508/\Delta F508}$ pigs were normal in appearance and lacked evidence of mucus accumulation. Like *CFTR*$^{-/-}$ pigs, on histopathological examination *CFTR*$^{\Delta F508/\Delta F508}$ airways lacked inflammatory cells (Fig. 1G) (25). The alveolar and airway epithelia were indistinguishable in *CFTR*$^{+/+}$, *CFTR*$^{\Delta F508/\Delta F508}$, and *CFTR*$^{-/-}$ pigs. Analysis of bronchoalveolar lavage of newborn pigs revealed no statistically significant differences in total cell counts, differential cell counts, or IL-8 concentrations between *CFTR*$^{+/+}$ and *CFTR*$^{\Delta F508/\Delta F508}$pigs (Fig. 1H–J).

Tracheal abnormalities occur in humans with CF and $CFTR^{-/-}$ pigs and mice (28,29). Compared to wild-type trachea, $CFTR^{\Delta F508/\Delta F508}$ trachea had an altered lumen area, circumference, submucosal gland area, and smooth muscle area (Fig. 2A–2E). However, changes in smooth muscle area were not as severe as those in $CFTR^{-/-}$ pigs.

Thus, newborn $CFTR^{\Delta F508/\Delta F508}$ pigs are remarkably similar to their $CFTR^{-/-}$ counterparts with the exception of slightly less severe abnormalities in pancreas and tracheal smooth muscle.

$CFTR^{\Delta F508/\Delta F508}$ lungs develop disease with time

Meconium ileus would prevent survival of all $CFTR^{\Delta F508/\Delta F508}$ pigs. Therefore, to learn whether disease in $CFTR^{\Delta F508/\Delta F508}$ pigs would progress after birth, surgical intervention was necessary to bypass the intestinal obstruction. Therefore, we placed an ileostomy or cecostomy in the pigs within 15 hr after birth. The procedures and treatments were the same as we previously described for $CFTR^{-/-}$pigs (25).

We examined the histopathology of four $CFTR^{\Delta F508/\Delta F508}$ pigs ranging in age from 13 to 87 days at time of euthanasia (Table 1). Over time, $CFTR^{\Delta F508/\Delta F508}$ pigs lost pancreatic parenchyma, which was replaced with fatty and fibrous tissue (Fig. 3A). In the liver, changes varied from minimal to diffuse steatosis (Fig. 3B,C). One animal (Case 2) had portal areas with focal to bridging fibrosis, duct proliferation and inflammation, the changes typical of progressive focal biliary cirrhosis (24) (Fig. 3D).

Like $CFTR^{-/-}$ and $CFTR^{\Delta F508/-}$ piglets (25), all the $CFTR^{\Delta F508/\Delta F508}$ pigs showed changes consistent with CF lung disease. Disease severity varied from animal to animal, and changes within lungs of individual pigs were heterogeneous such that some areas of lung showed no abnormality. As early as two weeks of age (Case 1), $CFTR^{\Delta F508/\Delta F508}$ lung showed mucopurulent material obstructing some airways with areas of adjacent atelectasis (Fig. 3E–H). In cases 2 and 4 (62 and 87 days old), lung changes included scattered mucopurulent debris in airway lumens with chronic purulent to lymphoid airway wall inflammation (Fig. 3I–L). The surface epithelium showed areas of goblet cell hyperplasia, and mucocellular material was detected in some submucosal glands. In case 3 (77 days old), the lungs showed a range of severity from nominal mucinous changes to lobular atelectasis consistent with airway obstruction (Fig. 3M).

At the time of necropsy, lung samples were aseptically removed for bacterial culture from three of the four animals. Bacteria were present in the cultures, but in relatively low numbers ranging from 10–1650 cfu/g lung tissue (Table 2). As in $CFTR^{-/-}$ pigs, a variety of bacterial species were isolated. This result suggests a host-defense defect for many bacterial species and is consistent with data from humans with early CF lung disease (25). In contrast, no bacteria were isolated from lungs of three of the four control pigs, and in the fourth only 10 cfu/g were cultured. In addition, $CFTR^{\Delta F508/\Delta F508}$ pigs, but not $CFTR^{+/+}$ pigs, received some systemic antibiotics (Materials and Methods), which may have suppressed bacterial recovery and minimized differences between the two groups.

These results indicate that $CFTR^{\Delta F508/\Delta F508}$ pigs spontaneously develop lung disease that resembles that in $CFTR^{-/-}$ pigs and humans homozygous for the *ΔF508* mutation.

$CFTR^{\Delta F508/\Delta F508}$ pigs produce $CFTR^{\Delta F508}$ mRNA

Because the phenotype of $CFTR^{\Delta F508/\Delta F508}$ pigs was like that of $CFTR^{-/-}$ pigs, we asked whether newborn $CFTR^{\Delta F508/\Delta F508}$ pigs produced *CFTR* transcripts. We assessed expression from the *ΔF508* allele using quantitative RT-PCR. Amounts of wild-type *CFTR* mRNA decreased from proximal to distal intestine and were lower in cultured airway

epithelia than in intestine (Fig. 4A). In $CFTR^{\Delta F508/\Delta F508}$ pig intestine, *CFTR* transcripts followed a similar axial pattern and did not statistically differ from those in $CFTR^{+/+}$ pigs. Northern blots of $CFTR^{\Delta F508/\Delta F508}$ duodenum were consistent with the RT-PCR data (Fig. 4B). In cultured airway epithelia, $CFTR^{+/+}$ and $CFTR^{\Delta F508/\Delta F508}$had the same abundance of CFTR transcripts. These data suggest that the Neo^R cassette in intron 10 has relatively minor effects on transcription from the $CFTR^{\Delta F508}$ allele. These results are also consistent with our earlier estimate that $CFTR^{\Delta F508}$ mRNA was present at ~70% of the wild-type amount (27).

The amount of CFTR-ΔF508 is reduced compared to wild-type CFTR

Processing of CFTR can be assessed by its migration on an SDS gel; immature CFTR (band B) has undergone core glycosylation in the endoplasmic reticulum (ER) and mature CFTR (band C) has been fully glycosylated in the Golgi complex (2,3). When expressed *in vitro*, most wild-type human CFTR migrates as band C, although a substantial amount of immature band B protein is also present. In human CFTR-ΔF508, band C is generally undetectable, and the predominance of band B indicates ER retention (2–4,26). In our earlier studies of recombinant porcine CFTR, wild-type protein behaved like wild-type human CFTR, whereas some of the mutant porcine protein processed to band C (26).

In proximal small intestine from wild-type pigs, we detected band C and very little band B CFTR (Fig. 4C). This result suggests that most wild-type protein was processed to the mature form, consistent with maturation of endogenous wild-type human CFTR to band C (30). Thus, presence of band B *in vitro* may be due to overexpression of recombinant protein. The amount of CFTR recovered from proximal $CFTR^{\Delta F508/\Delta F508}$ intestine was markedly reduced compared to $CFTR^{+/+}$ intestine, and we had to increase both the amount of protein studied and enhance the exposure to detect the mutant protein (Fig. 4C, lanes 2–7). Distal small intestine yielded similar results (Fig. 4C, lanes 9–12). In both cases, CFTR-ΔF508 was present in the mature band C and immature band B forms.

Because the intestine is affected by meconium ileus, we also assessed airway epithelia, which do not show secondary changes from the disease at birth. The data paralleled results from intestine. First, we detected little band B in either excised trachea (Fig. 4D, lanes 2–5) or differentiated cultures (lanes 8–10) of wild-type nasal epithelia; the preponderance of CFTR was in band C. Migration of band C protein was slightly slower than recombinant wild-type CFTR, suggesting some differences in glycosylation of CFTR *in vivo* compared to recombinant CFTR. Second, we detected both band B and band C forms of CFTR-ΔF508. Third, the amount of CFTR-ΔF508 protein was decreased compared to wild-type CFTR, although the reduction was less marked in cultured than excised epithelia.

These results agree with our earlier *in vitro* studies of recombinant porcine wild-type and ΔF508 CFTR (26). They suggest that porcine CFTR-ΔF508 has a biosynthetic defect. However, they also indicate that a fraction of the mutant protein is processed to the mature form.

Immunostaining reveals a reduced amount of CFTR-ΔF508

We used immunocytochemistry as an additional way to evaluate CFTR-ΔF508. In small intestine, we detected wild-type CFTR in the apical membrane of crypt, but not villus cells (Fig. 5A). In $CFTR^{\Delta F508/\Delta F508}$ intestine, we detected some immunostaining throughout the small intestine and the spiral colon. However, the signal was very weak and not uniformly detectable; the third panel of Fig. 5A shows an example in which we have electronically enhanced the CFTR (green) fluorescence so that the staining could be appreciated. $CFTR^{-/-}$ intestine had no immunostaining.

In excised trachea and differentiated primary cultures of nasal epithelia, wild-type CFTR localized almost exclusively at the apical membrane (Fig. 5B,C). In $CFTR^{\Delta F508/\Delta F508}$ tracheal tissue and cultures, immunostaining was barely detectable. In Fig. 5B, we show a rare example from $CFTR^{\Delta F508/\Delta F508}$ trachea where we detected CFTR and found it localized similarly to that in $CFTR^{+/+}$ trachea. For cultured $CFTR^{\Delta F508/\Delta F508}$ tracheal epithelia, we electronically amplified the signal post-collection to detect CFTR immunostaining that differed from that in wild-type cultured epithelia; staining extended from the apical membrane into the cytoplasm (Fig. 5C). We detected no CFTR immunostaining in excised or cultured $CFTR^{-/-}$ tracheal epithelia. The marked decrease in immunostaining in $CFTR^{\Delta F508/\Delta F508}$ intestinal crypts and airway epithelia is consistent with the greatly reduced amounts of CFTR recovered from these tissues. These data predicted that ion transport by $CFTR^{\Delta F508/\Delta F508}$ epithelia would be abnormal.

$CFTR^{\Delta F508/\Delta F508}$ airway epithelia show reduced but not absent CFTR Cl^- transport

We designed electrolyte transport studies to answer two questions. First, does transepithelial ion transport in newborn $CFTR^{\Delta F508/\Delta F508}$ airway epithelia differ from that in wild-type epithelia? Second, is Cl^- transport in $CFTR^{\Delta F508/\Delta F508}$ airway epithelia greater than that in $CFTR^{-/-}$ epithelia? We studied airway epithelia so that we could compare data to results from $CFTR^{-/-}$ pigs (31). We examined both nasal epithelia, which are often used to evaluate CF ion transport, and tracheal/bronchial epithelia because of their potential contribution to disease. We studied excised tissues as well as primary cultures of differentiated airway epithelia. We show data for excised tracheal epithelia in Fig. 6; the other data are in Fig. S1–S3.

Basal Vt and Isc did not differ between excised trachea from $CFTR^{\Delta F508/\Delta F508}$ and $CFTR^{+/+}$ pigs (Fig. 6). An inhibitor of epithelial Na^+ channels (100 μM apical amiloride) reduced Vt ($\Delta Vt_{amiloride}$) and Isc ($\Delta Isc_{amiloride}$) in $CFTR^{\Delta F508/\Delta F508}$ more than in wild-type epithelia. Our earlier work indicates that the greater $\Delta Vt_{amiloride}$ and $\Delta Isc_{amiloride}$ in CF epithelia is due to reduced CFTR anion conductance rather than greater Na^+ channel activity, and these data are consistent with that earlier study (31). Values of transepithelial electrical conductance (Gt) were large, probably because of “edge damage” associated with clamping epithelia in Ussing chambers (32) (compare with cultured epithelia in Fig. S2–S3). Amiloride reduced Gt ($\Delta Gt_{amiloride}$) to a similar extent in $CFTR^{\Delta F508/\Delta F508}$ and $CFTR^{+/+}$ epithelia.

In nasal epithelia, compared to wild-type, $CFTR^{\Delta F508/\Delta F508}$ epithelia had a greater basal Vt and $\Delta Vt_{amiloride}$ in culture and a greater basal Isc and $\Delta Isc_{amiloride}$ in excised epithelia (Fig. S1 and S2). These differences between CF and non-CF epithelia at the two locations are the result of differences between basal CFTR Cl^- channel activity and other epithelial properties rather than differences in rates of Na^+ transport (31). $\Delta Gt_{amiloride}$ in $CFTR^{\Delta F508/\Delta F508}$ nasal epithelia was less than or the same as that in wild-type epithelia consistent with the conclusion that Na^+ conductance is not greater in CF than non-CF epithelia (31). In excised and cultured nasal and tracheal/bronchial epithelia, these electrophysiological properties in $CFTR^{\Delta F508/\Delta F508}$ epithelia (Fig. 6, S1–S3) were approximately the same as those in $CFTR^{-/-}$ epithelia.

To assess CFTR function, we added 4,4′-diisothiocyanostilbene-2,2′-disulfonic acid (DIDS) to block non-CFTR Cl^- channels, followed by forskolin and IBMX to increase cellular concentrations of cAMP and phosphorylate and activate CFTR (33). In both tracheal/bronchial and nasal epithelia and in both excised tissue and cultured epithelia, the forskolin and IBMX- induced changes in Vt (ΔVt_{cAMP}), Isc (ΔIsc_{cAMP}), and Gt (ΔGt_{cAMP}) were markedly reduced in $CFTR^{\Delta F508/\Delta F508}$ compared to $CFTR^{+/+}$ epithelia (Fig. 6, S1–S3). Interestingly, for most of the electrophysiological measurements, there was either a

statistically significant difference or a non-significant trend for *CFTR*$^{\Delta F508/\Delta F508}$ epithelia to show more cAMP-stimulated Cl^- conductance and/or Cl^- transport than *CFTR*$^{-/-}$ epithelia. As an additional way of assessing CFTR-mediated Cl^- transport, after adding forskolin and IBMX, we applied GlyH-101, which inhibits CFTR Cl^- channels (34). The results paralleled what we found with cAMP-dependent stimulation; the response was markedly attenuated in *CFTR*$^{\Delta F508/\Delta F508}$ compared to wild-type epithelia, but often greater than in *CFTR*$^{-/-}$ epithelia.

In addition to Cl^-, CFTR also transports HCO_3^- (35,36), and it has been proposed that defective HCO_3^- transport may be critical for CF pathogenesis (37). Therefore, we also examined changes in Isc and Gt when tracheal epithelia were bathed in a Cl^--free HCO_3^- solution. Like the reduction in Cl^- conductance, HCO_3^-conductance was markedly reduced in *CFTR*$^{\Delta F508/\Delta F508}$ trachea (Fig. 7A,B).

Thus, the *ΔF508* allele greatly decreased both Cl^- and HCO_3^- conductances, consistent with a substantial loss of CFTR. However, compared to *CFTR*$^{-/-}$, *CFTR*$^{\Delta F508/\Delta F508}$ epithelia retained some apical CFTR function.

CFTR$^{\Delta F508/\Delta F508}$ epithelia have residual CFTR function

The finding that *CFTR*$^{\Delta F508\Delta F508}$ pigs develop lung disease and yet have some CFTR anion conductance provided us with an opportunity to begin to address the question of how much CFTR function is sufficient to prevent lung disease. As one assessment of residual CFTR function, we compared the forskolin and IBMX-induced increases in Isc (ΔIsc_{cAMP}) and Gt (ΔGt_{cAMP}) in the presence of amiloride and under short-circuit conditions (i.e., Vt clamped to zero and symmetrical solutions) (Fig. 6 and S1–3). In *CFTR*$^{\Delta F508/\Delta F508}$ excised and cultured nasal and tracheal/bronchial epithelia, the ΔIsc_{cAMP} was 9–15% of wild-type values (Table 3). Edge damage effects prevented accurate assessments of ΔGt_{cAMP} in excised epithelia, but in cultured epithelia, the *CFTR*$^{\Delta F508/\Delta F508}$ ΔGt_{cAMP} was 6–16% of *CFTR*$^{+/+}$ values. Although GlyH-101 can have effects in addition to inhibiting CFTR (38,39), we also calculated GlyH-101-induced changes (ΔIsc_{GlyH} and ΔGt_{GlyH}) and found that they varied from 3–32% in *CFTR*$^{\Delta F508/\Delta F508}$ epithelia compared to *CFTR*$^{+/+}$ epithelia. The mean of all these ΔIsc and ΔGt measurements was ~12% of values in *CFTR*$^{+/+}$ epithelia.

In addition to apical CFTR conductance, Isc and Gt are affected by other apical ion channels and basolateral membrane transport, and CFTR may be partially active before cAMP elevation. In addition, the relationship between CFTR conductance and Isc is not linear, and the percentage increase in Isc overestimates the amount of CFTR function (40,41). Therefore, we imposed a transepithelial Cl^- concentration gradient and measured the current response to basolateral membrane permeabilization with nystatin and addition of forskolin and IBMX (Fig. 7C,D). *CFTR*$^{\Delta F508/\Delta F508}$ nasal and tracheal epithelia generated 7–8% as much current as wild-type controls (Table 3). Subsequent addition of GlyH-101 produced a current change in *CFTR*$^{\Delta F508/\Delta F508}$ epithelia that was 2–8% of that in *CFTR*$^{+/+}$ epithelia (Fig. 7C,E). The mean of the changes in current was ~6% of values in *CFTR*$^{+/+}$ epithelia (Table 3).

These studies were done under conditions of maximal CFTR stimulation. Therefore, we also examined the response to increasing concentrations of forskolin and IBMX (at a fixed ratio of forskolin:IBMX of 1:10) (Fig. 7F,G). The EC50 for *CFTR*$^{+/+}$ epithelia was 0.07±0.01 μM forskolin. In contrast, the EC50 for forskolin in *CFTR*$^{\Delta F508/\Delta F508}$ epithelia was 0.60±0.19 μM.

Because forskolin and IBMX might generate different cellular cAMP concentrations in *CFTR*$^{\Delta F508/\Delta F508}$ and *CFTR*$^{+/+}$ epithelia, we repeated the experiments with 8-CPT-cAMP, a

membrane-permeable cAMP analog (Fig. 7H,I). The results were similar in that the EC50 in wild-type epithelia was 8.0±1.3 μM and in $CFTR^{\Delta F508/\Delta F508}$ it was 65.2±17.3 μM.

These results suggest that $CFTR^{\Delta F508/\Delta F508}$ epithelia have a reduced sensitivity to cAMP-dependent stimulation of Cl^- transport.

DISCUSSION

$CFTR^{\Delta F508/\Delta F508}$ pigs are born with gastrointestinal disease and spontaneously develop airway disease

Our earlier work showed that pigs lacking CFTR develop disease that mimics that in humans with CF (22,24,25,29). Here we found that pigs expressing the ΔF508 protein manifest a similar phenotype. Newborn $CFTR^{\Delta F508/\Delta F508}$ pigs exhibit CF gastrointestinal disease with meconium ileus, pancreatic destruction, early evidence of focal biliary cirrhosis, and microgallbladder. At birth, the lungs showed no evidence of inflammation. However, within weeks of birth, they developed lung disease like that in patients with CF.

In vitro studies of CFTR-ΔF508 predict *in vivo* function

Studies of human tissues expressing CFTR-ΔF508 have yielded varying and conflicting results about the behavior of CFTR-ΔF508 (12–20); those data have raised questions about whether the *in vitro* behavior of CFTR-ΔF508 predicts its behavior *in vivo*. Our earlier *in vitro* studies showed that although most porcine CFTR-ΔF508 is misprocessed and degraded, a fraction of the mutant protein matures and reaches the apical membrane where it generates a small Cl^- conductance (26). Our data in $CFTR^{\Delta F508/\Delta F508}$ pigs are consistent with those earlier studies. The total amount of CFTR was markedly reduced in $CFTR^{\Delta F508/\Delta F508}$ epithelia, consistent with substantial degradation (2–4). However, similar to *in vitro*, some CFTR-ΔF508 was processed to the mature form and trafficked to the apical membrane. As a result, $CFTR^{\Delta F508/\Delta F508}$ epithelia retained a small Cl^- conductance. These data indicate that *in vitro* studies of recombinant wild-type and ΔF508 porcine CFTR predict the behavior of the protein *in vivo*, a result important for biochemical experiments and drug discovery efforts.

Disease in $CFTR^{\Delta F508/\Delta F508}$ pigs is likely due to loss of CFTR function rather than misprocessing of the mutant protein

The autosomal recessive genetics of CF suggested that loss of CFTR function causes the disease. However, misfolded CFTR-ΔF508 has also been proposed to cause deleterious effects. Indeed, some *in vitro* studies showed that recombinant CFTR-ΔF508 could cause endoplasmic reticulum stress and an unfolded protein response, although these effects might have been due in part to over-expression (42,43).

Thus, we might have expected a more severe phenotype in $CFTR^{\Delta F508/\Delta F508}$ than $CFTR^{-/-}$ pigs if expression of CFTR-ΔF508 had an adverse effect. That was not the case. Although we did not test for endoplasmic reticulum stress, our data suggest that if it occurs in $CFTR^{\Delta F508/\Delta F508}$ pigs, it is not likely to markedly worsen the disease. However, we also note that our studies were done on newborn pigs, and it would be interesting to test for an unfolded protein response in older animals.

Residual CFTR function in $CFTR^{\Delta F508/\Delta F508}$ pigs attenuates pancreatic and tracheal abnormalities

Our biochemical, immunostaining, and electrophysiological studies of excised and cultured epithelia all indicate that a fraction of porcine CFTR-ΔF508 escapes misprocessing and retains some Cl^- channel function. Although this residual CFTR activity was not sufficient

to prevent disease, it did impact severity in the pancreas and trachea. Pancreas is an organ that shows a strong correlation between *CFTR* genotype and phenotype in humans (1,44), and interestingly, pancreatic destruction was slightly less severe in $CFTR^{\Delta F508/\Delta F508}$ than $CFTR^{-/-}$ pigs. In addition, the changes in tracheal smooth muscle were less marked in $CFTR^{\Delta F508/\Delta F508}$ than $CFTR^{-/-}$ pigs. In contrast, we did not discern a milder or more severe phenotype in the intestine, liver, gallbladder, or lung of the $CFTR^{\Delta F508/\Delta F508}$ compared to $CFTR^{-/-}$ animals. However, heterogeneity of disease within those individual organs, variations in severity between animals, and difficulty in quantitating severity could have obscured minor differences.

Residual CFTR function in $CFTR^{\Delta F508/\Delta F508}$ pigs is not sufficient to prevent lung disease

Discovery that CFTR-ΔF508 is partially processed and functional in $CFTR^{\Delta F508/\Delta F508}$ pigs allowed us to begin to address a persistent question; how much CFTR activity is required to maintain a normal lung? Our results point to two relevant factors.

First, measuring cAMP-stimulated elevations and GlyH-101-induced inhibitions of Gt and Isc indicated that $CFTR^{\Delta F508/\Delta F508}$ epithelia generated ~12% as much conductance and current as wild-type epithelia. Measurements of CFTR Cl^- current after basolateral membrane permeabilization suggested that $CFTR^{\Delta F508/\Delta F508}$ epithelia had ~6% as much current as wild-type epithelia. These analyses have several advantages. We were able to compare electrophysiological data to those in $CFTR^{-/-}$ pigs, thereby identifying CFTR-specific properties. By studying newborns, we could eliminate confounding effects of infection, inflammation and remodeling. We also made measurements in both excised and cultured epithelia, and in both nasal and tracheal epithelia.

Second, our data revealed that cAMP-dependent stimulation was less potent at increasing Isc in $CFTR^{\Delta F508/\Delta F508}$ than $CFTR^{+/+}$ epithelia. Thus, under physiological conditions, where stimuli are unlikely to be maximal, the relative activity of CFTR-ΔF508 may be substantially less than ~6% of apical CFTR conductance or ~12% of Isc and Gt that we calculated for maximal stimulation. Hence, estimates based solely on studies with maximal stimulation may overestimate actual activity under more physiological conditions. That said, it is currently not possible to know where “physiological” conditions lie on the dose-response curve. The mechanisms responsible for the altered relationship between stimulation and CFTR activity are also unknown. However in *Xenopus* oocytes, CFTR-ΔF508 was ~10-fold less potently stimulated by cAMP elevation than wild-type CFTR (45). In addition, studies of CFTR-ΔF508 in membrane patches have reported either a slower apparent PKA-dependent activation rate or an accelerated inactivation rate (46,47). Additional studies seem warranted to investigate these phenomena.

The quantitative relationship between CFTR-mediated anion transport and lung disease has been difficult to elucidate without a model that develops typical pulmonary disease. The fact that humans who are heterozygotes for *CFTR* gene mutations do not have disease suggests that ~50% of *CFTR* mRNA is sufficient to prevent airway disease. A study using nested RT-PCR identified four individuals who did not have CF-like lung disease and had an estimated 8–27% of wild-type *CFTR* mRNA (48). In addition, it has been suggested that 20% of wild-type CFTR Cl^- current rescues the intestinal phenotype of *CFTR-null* mice (49). Other studies found that ~20% of wild-type cells or CF epithelia containing ~10% of CFTR overexpressing cells generated 70–80% of the Cl^- transport of wild-type airway epithelia, although the relationship to clinical disease could not be tested (40,41). Our studies set a value above which anion transport will be required to rescue the pulmonary phenotype in CF pigs; how much higher that value is, we do not know. However, some caveats are worth considering. These estimates are derived from $CFTR^{\Delta F508/\Delta F508}$ pigs and not humans with a *ΔF508* allele; lung disease might be more or less severe in pigs than humans. In addition,

modifier genes and Ca^{2+}-activated Cl^- channels might differ between pigs and humans. Environmental factors will also differ between the species; humans are exposed to respiratory viral infections, whereas such exposures are minimal for pigs in our animal care unit. Nevertheless, the striking similar lung disease between the two species suggests that similar pathogenic mechanisms are responsible.

In conclusion, our data indicate that CFTR-ΔF508 is misprocessed in pigs, and this produces a clinical phenotype that is strikingly similar to that in *CFTR*$^{-/-}$ pigs and humans with CF. These animals might be beneficial for investigating mechanisms of CFTR-ΔF508 biosynthesis *in vivo*, for understanding pathogenesis, and for assessing therapeutics to prevent lung disease. Finally, our results suggest strategies to further determine the amount of CFTR function required to prevent disease.

Supplementary Material

Refer to Web version on PubMed Central for supplementary material.

Acknowledgments

We thank Pamela Hughes, Ping Tan, Theresa Mayhew, and Paul Naumann for excellent assistance. We thank Dr. Kathryn Chaloner for statistical advice. GlyH-101 was a generous gift from the Cystic Fibrosis Foundation Therapeutics and R. Bridges. This work was supported by the NIH (HL51670, HL091842, DK54759) and Cystic Fibrosis Foundation. DAS was supported by AI076671. MJW is an Investigator of the HHMI. MJW was a co-founder of Exemplar Genetics, a company licensing materials and technology related to this work.

References

1. Welsh, MJ.; Ramsey, BW.; Accurso, F.; Cutting, GR. Cystic Fibrosis. In: Scriver, CR., et al., editors. The Metabolic and Molecular Basis of Inherited Disease. McGraw-Hill; New York: 2001. p. 5121-5189.
2. Cheng SH, et al. Defective intracellular transport and processing of CFTR is the molecular basis of most cystic fibrosis. Cell. 1990; 63:827–834. [PubMed: 1699669]
3. Ward CL, Kopito RR. Intracellular turnover of cystic fibrosis transmembrane conductance regulator. Inefficient processing and rapid degradation of wild-type and mutant proteins. J Biol Chem. 1994; 269(41):25710–25718. [PubMed: 7523390]
4. Younger JM, et al. Sequential quality-control checkpoints triage misfolded cystic fibrosis transmembrane conductance regulator. Cell. 2006; 126(3):571–582. [PubMed: 16901789]
5. Denning GM, et al. Processing of mutant cystic fibrosis transmembrane conductance regulator is temperature-sensitive. Nature. 1992; 358:761–764. [PubMed: 1380673]
6. Haws CM, et al. ΔF508-CFTR channels: kinetics, activation by forskolin, and potention by xanthines. Am J Physiol. 1996; 270:C1544–C1555. [PubMed: 8967457]
7. Cholon DM, O'Neal WK, Randell SH, Riordan JR, Gentzsch M. Modulation of endocytic trafficking and apical stability of CFTR in primary human airway epithelial cultures. Am J Physiol Lung Cell Mol Physiol. 2010; 298(3):L304–314. [PubMed: 20008117]
8. Jurkuvenaite A, et al. Functional stability of rescued delta F508 cystic fibrosis transmembrane conductance regulator in airway epithelial cells. Am J Respir Cell Mol Biol. 2010; 42(3):363–372. [PubMed: 19502384]
9. Okiyoneda T, et al. Peripheral protein quality control removes unfolded CFTR from the plasma membrane. Science. 2010; 329(5993):805–810. [PubMed: 20595578]
10. Pedemonte N, et al. Small-molecule correctors of defective DeltaF508-CFTR cellular processing identified by high-throughput screening. J Clin Invest. 2005; 115(9):2564–2571. [PubMed: 16127463]
11. Van Goor F, et al. Rescue of ΔF508-CFTR trafficking and gating in human cystic fibrosis airway primary cultures by small molecules. Am J Physiol Lung Cell Mol Physiol. 2006; 290(6):L1117–11130. [PubMed: 16443646]

12. Kalin N, Claaß A, Sommer M, Puchelle E, Tummler B. ΔF508 CFTR protein expression in tissues from patients with cystic fibrosis. J Clin Invest. 1999; 103(10):1379–1389. [PubMed: 10330420]
13. van Barneveld A, et al. Functional analysis of F508del CFTR in native human colon. Biochim Biophys Acta. 2010; 1802:1062–1069. [PubMed: 20696241]
14. Dupuit F, et al. CFTR and differentiation markers expression in non-CF and ΔF508 homozygous CF nasal epithelium. J Clin Invest. 1995; 96:1601–1611. [PubMed: 7544810]
15. Penque D, et al. Cystic fibrosis F508del patients have apically localized CFTR in a reduced number of airway cells. Lab Invest. 2000; 80(6):857–868. [PubMed: 10879737]
16. Kartner N, Augustinas O, Jensen TJ, Naismith AL, Riordan JR. Mislocalization of ΔF508 CFTR in cystic fibrosis sweat gland. Nat Genet. 1992; 1:321–327. [PubMed: 1284548]
17. Engelhardt JF, et al. Submucosal glands are the predominant site of CFTR expression in the human bronchus. Nat Genet. 1992; 2:240–248. [PubMed: 1285365]
18. Kreda SM, et al. Characterization of wild-type and deltaF508 cystic fibrosis transmembrane regulator in human respiratory epithelia. Mol Biol Cell. 2005; 16(5):2154–2167. [PubMed: 15716351]
19. Sermet-Gaudelus I, et al. Normal function of the cystic fibrosis conductance regulator protein can be associated with homozygous (Delta)F508 mutation. Pediatr Res. 2002; 52(5):628–635. [PubMed: 12409506]
20. Ho LP, et al. Correlation between nasal potential difference measurements, genotype and clinical condition in patients with cystic fibrosis. Eur Respir J. 1997; 10(9):2018–2022. [PubMed: 9311495]
21. Grubb BR, Boucher RC. Pathophysiology of gene-targeted mouse models for cystic fibrosis. Physiol Rev. 1999; 79(Suppl 1):S193–S214. [PubMed: 9922382]
22. Rogers CS, et al. Disruption of the CFTR gene produces a model of cystic fibrosis in newborn pigs. Science. 2008; 321(5897):1837–1841. [PubMed: 18818360]
23. Sun X, et al. Disease phenotype of a ferret CFTR-knockout model of cystic fibrosis. J Clin Invest. 2010; 120(9):3149–3160. [PubMed: 20739752]
24. Meyerholz DK, Stoltz DA, Pezzulo AA, Welsh MJ. Pathology of gastrointestinal organs in a porcine model of cystic fibrosis. Am J Pathol. 2010; 176(3):1377–1389. [PubMed: 20110417]
25. Stoltz DA, et al. Cystic fibrosis pigs develop lung disease and exhibit defective bacterial eradication at birth. Science Translational Medicine. 2010; 2(29):29ra31 .
26. Ostedgaard LS, et al. Processing and function of CFTR-ΔF508 are species-dependent. Proc Natl Acad Sci U S A. 2007; 104(39):15370–15375. [PubMed: 17873061]
27. Rogers CS, et al. Production of CFTR null and ΔF508 heterozygous pigs by AAV-mediated gene targeting and somatic cell nuclear transfer. J Clin Invest. 2008; 118(4):1571–1577. [PubMed: 18324337]
28. Bonvin E, et al. Congenital tracheal malformation in cystic fibrosis transmembrane conductance regulator-deficient mice. J Physiol. 2008; 586(13):3231–3243. [PubMed: 18450781]
29. Meyerholz DK, et al. Loss of CFTR function produces abnormalities in tracheal development in neonatal pigs and young children. Am J Respir Crit Care Med. 2010; 182:1251–1261. [PubMed: 20622026]
30. Varga K, et al. Efficient intracellular processing of the endogenous cystic fibrosis transmembrane conductance regulator in epithelial cell lines. J Biol Chem. 2004; 279(21):22578–22584. [PubMed: 15066992]
31. Chen JH, et al. Loss of anion transport without increased sodium absorption characterize newborn porcine cystic fibrosis airway epithelia. Cell. 2010; 143:911–923. [PubMed: 21145458]
32. Helman SI, Miller DA. Edge damage effect on electrical measurements of frog skin. Am J Physiol Cell Physiol. 1973; 225(4):972–977.
33. Sheppard DN, Welsh MJ. Structure and function of the CFTR Cl^- channel. Physiol Rev. 1999; 79(1):S23–S45. [PubMed: 9922375]
34. Muanprasat C, et al. Discovery of glycine hydrazide pore-occluding CFTR inhibitors: mechanism, structure-activity analysis, and in vivo efficacy. J Gen Physiol. 2004; 124(2):125–137. [PubMed: 15277574]

35. Poulsen JH, Fischer H, Illek B, Machen TE. Bicarbonate conductance and pH regulatory capability of cystic fibrosis transmembrane conductance regulator. Proc Natl Acad Sci U S A. 1994; 91(12): 5340–5344. [PubMed: 7515498]
36. Smith JJ, Welsh MJ. cAMP stimulates bicarbonate secretion across normal, but not cystic fibrosis airway epithelia. J Clin Invest. 1992; 89:1148–1153. [PubMed: 1313448]
37. Quinton PM. Cystic fibrosis: impaired bicarbonate secretion and mucoviscidosis. Lancet. 2008; 372(9636):415–417. [PubMed: 18675692]
38. Kelly M, et al. Cystic fibrosis transmembrane regulator inhibitors $CFTR_{inh}$-172 and GlyH-101 target mitochondrial functions, independently of chloride channel inhibition. J Pharmacol Exp Ther. 2010; 333(1):60–69. [PubMed: 20051483]
39. Caputo A, et al. TMEM16A, a membrane protein associated with calcium-dependent chloride channel activity. Science. 2008; 322(5901):590–594. [PubMed: 18772398]
40. Farmen SL, et al. Gene transfer of CFTR to airway epithelia: low levels of expression are sufficient to correct Cl^- transport and overexpression can generate basolateral CFTR. Am J Physiol Lung Cell Mol Physiol. 2005; 280:L1123–1130. [PubMed: 16085675]
41. Johnson LG, et al. Efficiency of gene transfer for restoration of normal airway epithelial function in cystic fibrosis. Nat Genet. 1992; 2:21–25. [PubMed: 1284642]
42. Bartoszewski R, et al. Activation of the unfolded protein response by deltaF508 CFTR. Am J Respir Cell Mol Biol. 2008; 39(4):448–457. [PubMed: 18458236]
43. Hybiske K, et al. Effects of cystic fibrosis transmembrane conductance regulator and DeltaF508CFTR on inflammatory response, ER stress, and Ca^{2+} of airway epithelia. Am J Physiol Lung Cell Mol Physiol. 2007; 293(5):L1250–1260. [PubMed: 17827250]
44. Wilschanski M, Durie PR. Pathology of pancreatic and intestinal disorders in cystic fibrosis. J R Soc Med. 1998; 91(Suppl 34):40–49. [PubMed: 9709387]
45. Drumm ML, et al. Chloride conductance expressed by ΔF508 and other mutant CFTRs in *Xenopus* oocytes. Science. 1991; 254:1797–1799. [PubMed: 1722350]
46. Wang F, Zeltwanger S, Hu S, Hwang TC. Deletion of phenylalanine 508 causes attenuated phosphorylation-dependent activation of CFTR chloride channels. J Physiol. 2000; 524(Pt 3):637–648. [PubMed: 10790148]
47. Schultz BD, Frizzell RA, Bridges RJ. Rescue of dysfunctional ΔF508-CFTR chloride channel activity by IBMX. J Membr Biol. 1999; 170(1):51–66. [PubMed: 10398760]
48. Chu CS, Trapnell BC, Curristin SM, Cutting GR, Crystal RG. Extensive posttranscriptional deletion of the coding sequences for part of nucleotide-binding fold 1 in respiratory epithelial mRNA transcripts of the cystic fibrosis transmembrane conductance regulator gene is not associated with the clinical manifestations of cystic fibrosis. J Clin Invest. 1992; 90:785–790. [PubMed: 1381723]
49. Dorin JR, et al. A demonstration using mouse models that successful gene therapy for cystic fibrosis requires only partial gene correction. Gene Ther. 1996; 3(9):797–801. [PubMed: 8875228]

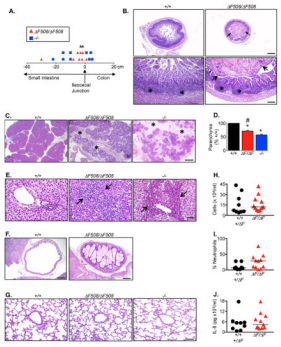

Figure 1. Pathology of newborn *CFTR*$^{\Delta F508/\Delta F508}$ pigs

A. Location (in cm) of meconium ileus obstruction in *CFTR*$^{\Delta F508/\Delta F508}$ (n=10) and *CFTR*$^{-/-}$ (n=9) pigs.

B. *CFTR*$^{\Delta F508/\Delta F508}$ileum distal to the obstruction had a small caliber and was heterogeneously filled with mucocellular debris (arrows). Ileal Peyer's patches (asterisks) appeared similar in CFTR$^{+/+}$ and *CFTR*$^{\Delta F508/\Delta F508}$ pigs. Bars=725 top and 145 μm bottom.

C. Pancreas from *CFTR*$^{\Delta F508/\Delta F508}$ pigs had increased connective tissue (asterisks) and destruction compared to *CFTR*$^{+/+}$. Histopathological changes in *CFTR*$^{\Delta F508/\Delta F508}$ pancreas were slightly less severe than in *CFTR*$^{-/-}$. HE stain. Bar=457 μm.

D. Lobular parenchyma in *CFTR*$^{\Delta F508/\Delta F508}$ pigs (n=17) was reduced compared to *CFTR*$^{+/+}$ (n=9, * $P<0.001$) and greater than in *CFTR*$^{-/-}$ (n=19, # $P<0.05$, Dunn's post-test). Data from *CFTR*$^{+/+}$ and *CFTR*$^{-/-}$ pigs were previously published (24).

E. Liver from newborn *CFTR*$^{\Delta F508/\Delta F508}$and *CFTR*$^{-/-}$ pigs showed portal areas that were focally expanded (arrows) by inflammation, duct proliferation and connective tissue. HE stain. Bar=46 μm.

F. *CFTR*$^{\Delta F508/\Delta F508}$ pigs had microgallbladder variably filled by mucus and bile. HE stain, bars=928 μm (+/+) and 463 μm (*ΔF508/ΔF508*).

G. Lung from newborn *CFTR*$^{\Delta F508/\Delta F508}$ pigs lacked mucus accumulation or inflammatory changes. HE stain. Bar=93 μm.

H–J. Bronchoalveolar lavage liquid analyses from newborn pigs, including total cell counts (**H**), neutrophil percentages (**I**), and IL-8 concentrations (**J**) revealed no statistically significant differences between genotypes. *CFTR*$^{+/+}$ (n=5) combined with *CFTR*$^{+/\Delta F508}$ (n=4); *CFTR*$^{\Delta F508/\Delta F508}$ (n=11).

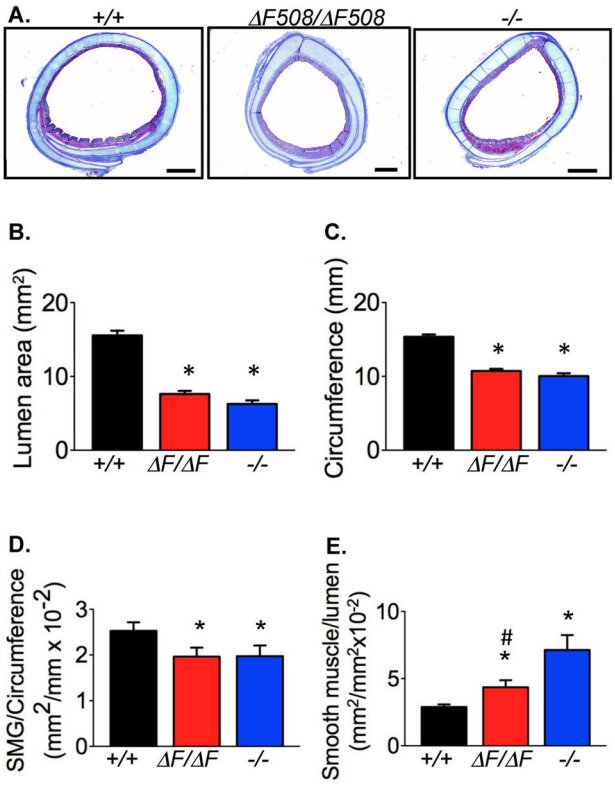

Figure 2. Morphometry of newborn *CFTR*$^{\Delta F508/\Delta F508}$ trachea

A. Cross section of trachea. MT stain. Bars=1 mm. Images from CFTR$^{+/+}$ and *CFTR*$^{-/-}$ are from reference (29).

B–E. Tracheal morphometry in *CFTR*$^{+/+}$ (n=20), *CFTR*$^{\Delta F508/\Delta F508}$ (n=19), and *CFTR*$^{-/-}$ (n=18) newborn pigs. * indicates different from *CFTR*$^{+/+}$ and # indicates different from *CFTR*$^{-/-}$ (* $P<0.05$ *vs. CFTR*$^{+/+}$, and # $P<0.05$ *vs. CFTR*$^{-/-}$, 1-way ANOVA with Bonferroni's post test).

B. Tracheal lumen cross-sectional area.

C. Tracheal circumference.

D. Submucosal gland area normalized to tracheal lumen circumference.

E. Smooth muscle area normalized to tracheal lumen area.

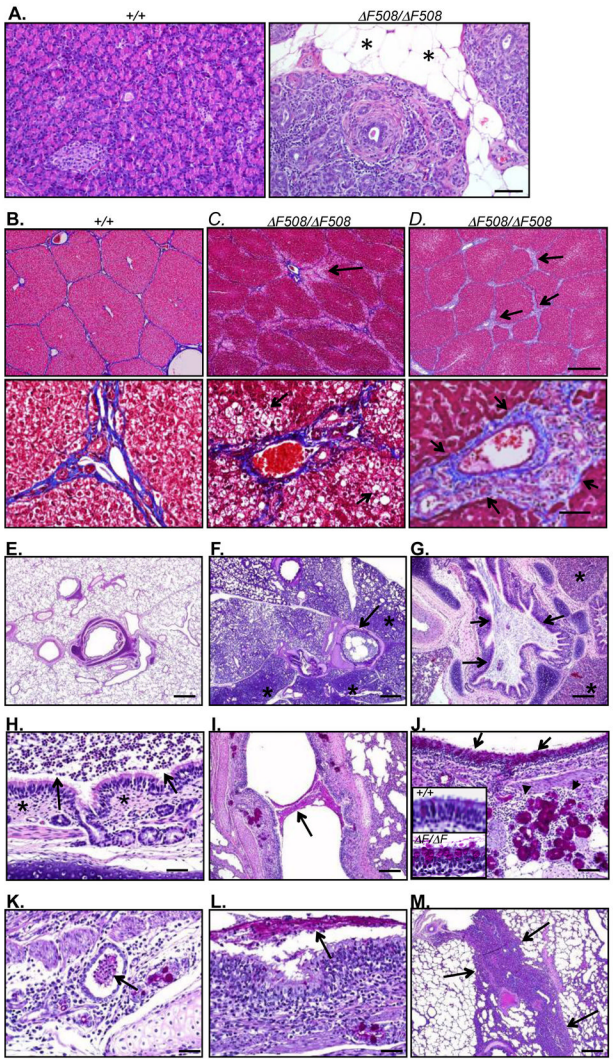

Figure 3. Disease progression in pigs ~2-weeks of age and older

A. Pancreas from a 77-day old *CFTR*$^{\Delta F508/\Delta F508}$ pig and 69-day old *CFTR*$^{+/+}$ pig for comparison. Islands of degenerative, fibrotic and inflamed *CFTR*$^{\Delta F508/\Delta F508}$ pancreas were surrounded by abundant adipose tissue (asterisk). HE stain. Bar=75 μm.

B–D. Porcine liver. MT stain. Bars=570 top and 57 μm bottom. **B.** Liver from a 136-day old *CFTR*$^{+/+}$ pig. C. Diffuse zone 1 steatosis (black arrows) in a 77-day old *CFTR*$^{\Delta F508/\Delta F508}$ pig. **D.** A 62-day old *CFTR*$^{\Delta F508/\Delta F508}$ pig had focal to bridging expansion (black arrows) of triads by fibrosis, duct proliferation and inflammation.

E–M. Histopathological evaluation of *CFTR*$^{\Delta F508/\Delta F508}$ lungs. **E–H** are HE stain and **I–M** are PAS stain.

E. Lung from a 69-day old *CFTR*$^{+/+}$ pig; changes like those in panels F–H were not observed in wild-type pigs.

F–H. Lung from 13-day old *CFTR*$^{\Delta F508/\Delta F508}$ pig.

F. Lungs showed mucopurulent airway obstruction (arrow) and adjacent atelectasis (asterisks). Bar=757 μm.

G. Affected airway lumens often contained a heterogeneous mixture of mucopurulent debris obstructing the airway (arrows) and adjacent atelectasis (asterisks). Bar = 378 μm.

H. Airways sometimes showed nominal inflammatory changes in the wall (asterisks) adjacent to luminal neutrophils (arrows) suggesting the dispersion of the luminal mucocellular debris from more severely affected airways. Bar=38 μm.
I–J. Lung from 87-day old *CFTR*$^{\Delta F508/\Delta F508}$ pig.
I. Some airways showed focal airway mucus obstruction (arrow). Bar=162 μm.
J. The surface epithelium showed focal goblet cell hyperplasia (black arrows) and inflammation in the airway wall around submucosal glands (arrowheads). Bar=81 μm. Insets: magnified PAS-stained images of airway epithelia of 4.5-mo *CFTR*$^{+/+}$ (top) and 87-day *CFTR*$^{\Delta F508/\Delta F508}$ (bottom) pigs.
K–L. Lung from 62-day old *CFTR*$^{\Delta F508/\Delta F508}$ pig.
K. Lungs showed mucopurulent inflammation associated with focal dilated submucosal glands and ducts (arrow). Bar=40 μm.
L. Airway lumens showed mucopurulent material in lumen (arrow) with epithelial proliferation and wall inflammation. Bar=40 μm.
M. Lung from 77-day old pig showed lesions included complete lobular atelectasis (arrows), although in this image airway obstruction was not present. Bar=378 μm.

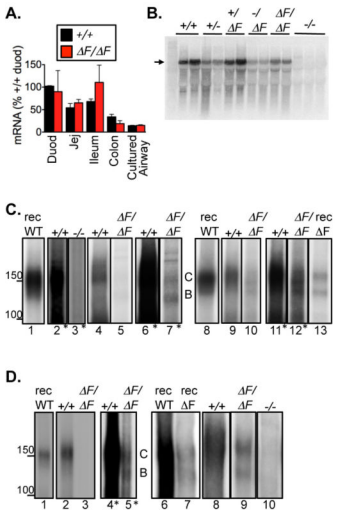

Figure 4. mRNA and protein expression in intestine and airway

A. Quantitative RT-PCR of *CFTR* mRNA in *CFTR*$^{\Delta F508/\Delta F508}$ and *CFTR*$^{+/+}$ pigs. Data are from triplicate assays repeated on multiple days. For each tissue, amounts of *CFTR* mRNA were normalized to β-actin mRNA. These normalized values were then expressed relative to that in wild-type duodenum. Data are mean±SE from intestinal tissues from 6 *CFTR*$^{+/+}$ and 6 *CFTR*$^{\Delta F508/\Delta F508}$piglets, and from cultured nasal epithelia from 1 *CFTR*$^{+/+}$ piglet (n=3) and 1 *CFTR*$^{\Delta F508/\Delta F508}$piglet (n=4).

B. Northern blot analysis of duodenal *CFTR* mRNA, indicated by arrow.

C. Immunoprecipitated and *in vitro* phosphorylated CFTR isolated from intestine. “rec” (lanes 1,8,13) indicates recombinant protein. Lanes 2–7, proximal intestine. CFTR$^{+/+}$ and *CFTR*$^{-/-}$ 500 μg and *CFTR*$^{\Delta F508/\Delta F508}$ 750 μg. Lanes marked with * show enhanced exposure. Lanes 6 and 7 are same as lanes 4 and 5. Lanes 9–12, distal intestine. CFTR$^{+/+}$ 200 μg and *CFTR*$^{\Delta F508/\Delta F508}$ 1000 μg. Lanes 11 and 12 are same as 9 and 10.

D. Immunoprecipitated and *in vitro* phosphorylated CFTR isolated from airway epithelia. Recombinant protein, lanes 1,6,7. Lanes 2–5, trachea; CFTR$^{+/+}$ 623 μg and *CFTR*$^{\Delta F508/\Delta F508}$ 1208 μg. Lanes 4 and 5 are same as lanes 2 and 3. Lanes 8–10, cultured bronchial epithelia; each lane 750 μg.

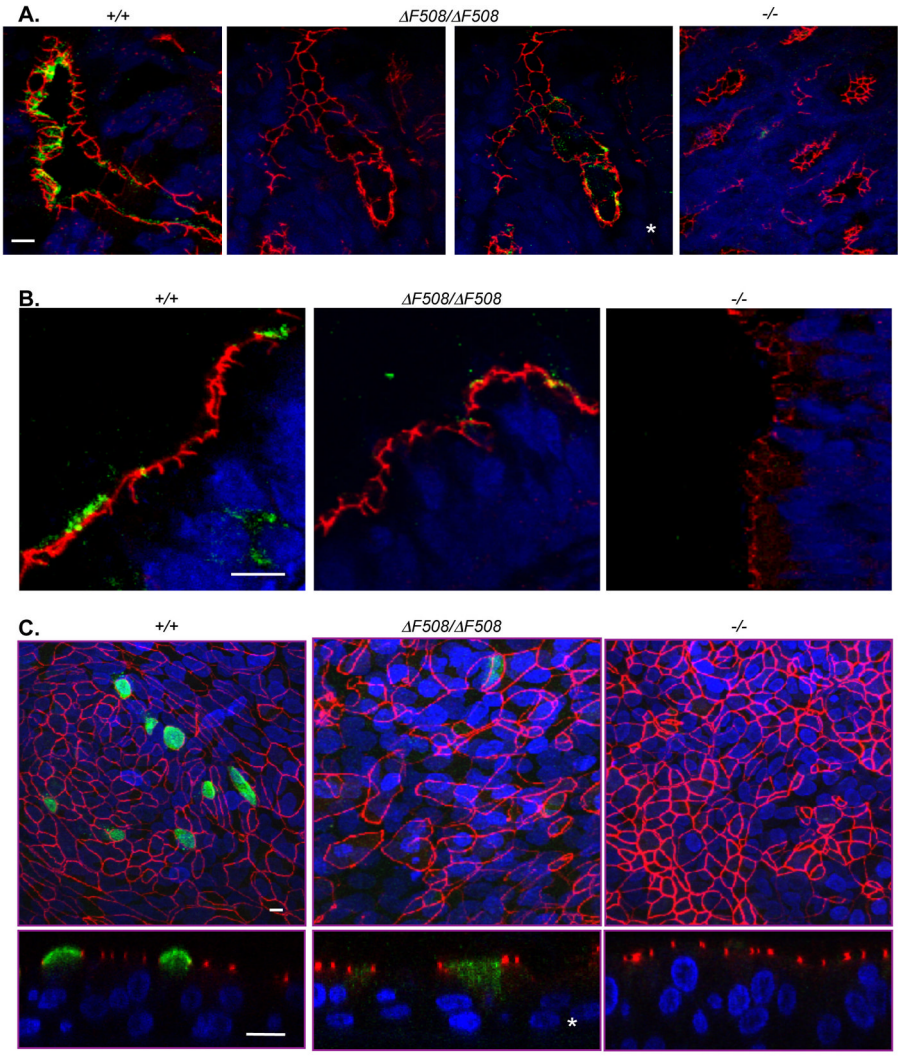

Figure 5.

Immunocytochemical localization of CFTR in intestinal and airway epithelia of newborn pigs. Data are stacks of confocal images, except as noted. Scale bars=10 μm.

A. Sections of intestine from newborn pigs. Third panel (asterisk) shows an electronically enhanced image of second panel. CFTR is green, ZO-1 is red, and nuclei are blue. Nonspecific staining was occasionally found in lumen of some $CFTR^{\Delta F508/\Delta F508}$and $CFTR^{-/-}$ crypts in areas of extensive mucus.

B. Sections of trachea.

C. Images of cultured airway epithelia. Top panels are enface images, and bottom panels are single vertical sections. Images from $CFTR^{\Delta F508\Delta F508}$ epithelia are electronically enhanced (*) to show CFTR. Cell size heterogeneity was observed with all genotypes.

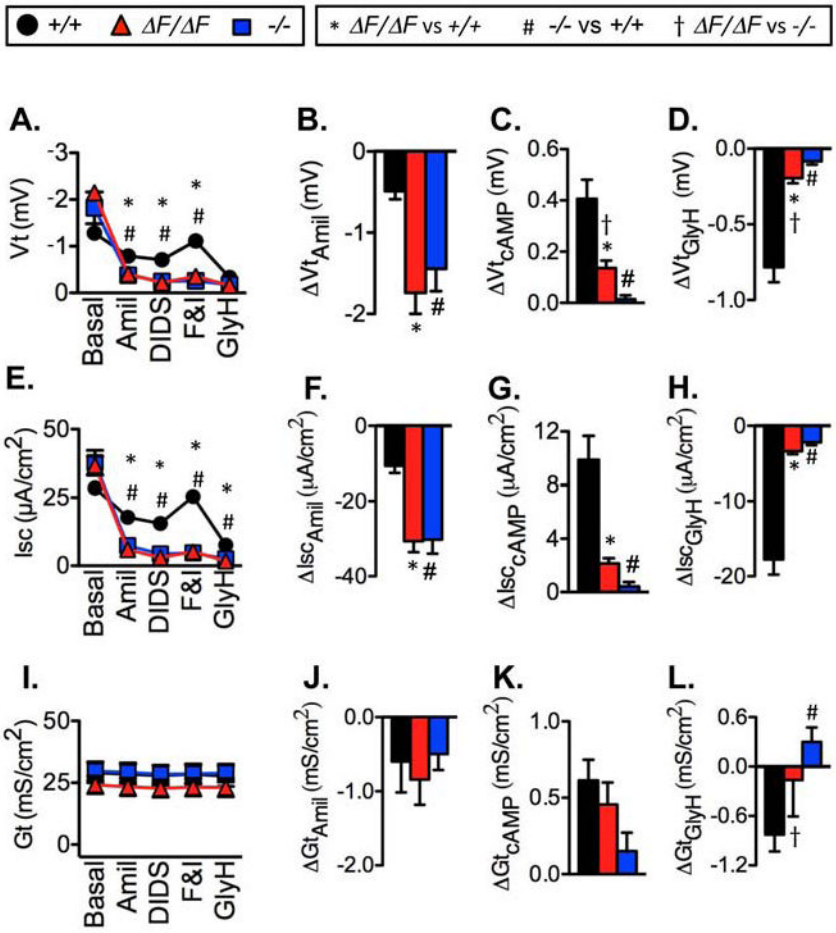

Figure 6.

Electrophysiological properties of freshly excised porcine tracheal epithelia. Data are from $CFTR^{+/+}$(23 tissues, 23 pigs), $CFTR^{\Delta F508/\Delta F508}$ (19 tissues, 17 pigs), and $CFTR^{-/-}$(16 tissues, 14 pigs) epithelia. Data from $CFTR^{-/-}$ and most CFTR $^{+/+}$ pigs were previously reported(31). * indicates $CFTR^{\Delta F508/\Delta F508}$ differs from $CFTR^{+/+}$, # indicates $CFTR^{-/-}$ differs from $CFTR^{+/+}$, and † indicates $CFTR^{\Delta F508/\Delta F508}$ differs from $CFTR^{-/-}$, all at P<0.017 by unpaired t test with Welch's correction.

A). Transepithelial voltage (Vt) and response to sequential apical addition of 100 μM amiloride, 100 μM DIDS, 10 μM forskolin and 100 μM IBMX, and 100 μM GlyH-101.

B). ΔVt_{amil} indicates change in Vt with addition of amiloride.

C). ΔVt_{cAMP} indicates change in Vt with addition of forskolin and IBMX.

D). ΔVt_{GlyH} indicates change in Vt with addition of GlyH-101.

E–H). Short-circuit current (Isc) measurements corresponding to Vt measurements in panels A–D.

I–L). Transepithelial conductance (Gt) measurements corresponding to Vt measurements in panels A–D. Changes in Vt, Isc, and Gt with DIDS were small and did not differ by genotype.

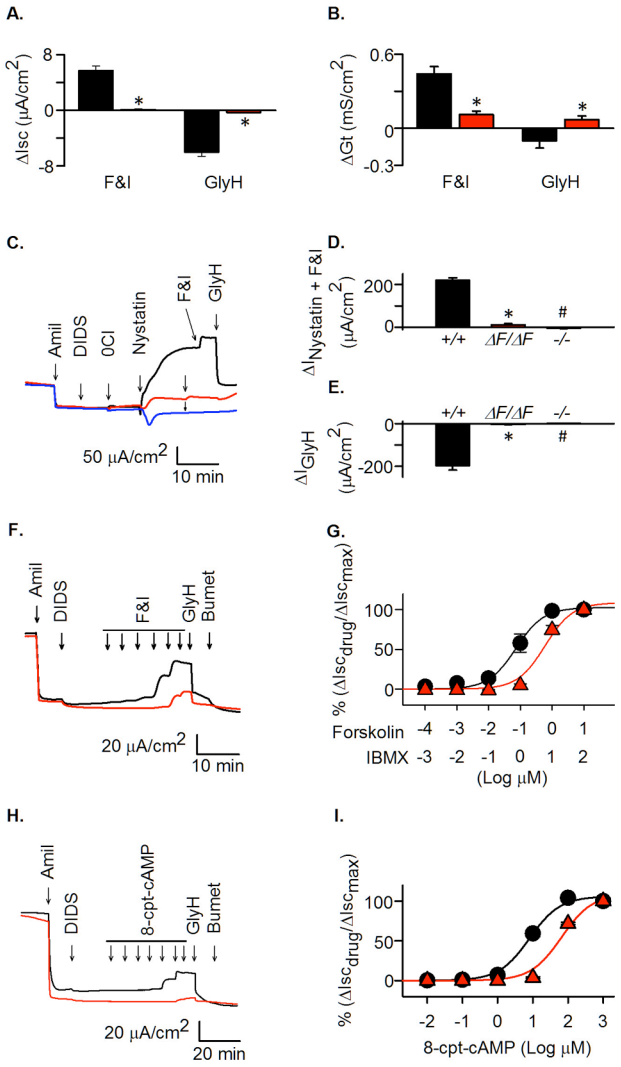

Figure 7. HCO_3^- transport, apical Cl^- currents, and effect of increasing cAMP-dependent stimulation

A–B. Changes in Isc and Gt in tracheal epithelia bathed in Cl^--free solution containing 25 mM HCO_3^-. Change in Isc (ΔIsc) (A) and Gt (ΔGt) (B). stimulated by forskolin (10 μM) and IBMX (100 μM) (F&I) and inhibited by GlyH-101 (100 μM, apical). * indicates $P < 0.05$, unpaired t- test. N=7 $CFTR^{+/+}$and 7 $CFTR^{\Delta F508/\Delta F508}$.

C–E Changes in Cl^- current after permeabilization of basolateral membrane. N=7 $CFTR^{+/+}$and 7 $CFTR^{\Delta F508/\Delta F508}$.

C). Current traces in response to indicated agents in $CFTR^{+/+}$, $CFTR^{\Delta F508/\Delta F508}$, and $CFTR^{-/-}$ epithelia. Concentrations are those indicated in Fig. 6 legend; nystatin was 0.36 mg/ml.

D). Change in current in response to nystatin plus forskolin and IBMX ($\Delta I_{Nystatin+F\&I}$).

E). Change in current in response to GlyH-101 (ΔI_{GlyH}).

F). Examples of Isc current traces following addition of increasing forskolin and IBMX concentrations. For concentrations, see panel G.

G). Changes in Isc with increasing forskolin and IBMX concentrations. N=7 $CFTR^{+/+}$and 6 $CFTR^{\Delta F508/\Delta F508}$.

H). Examples of Isc current traces following addition of increasing 8-cpt-cAMP concentrations. For concentrations, see panel I.

I). Changes in Isc with increasing 8-cpt-cAMP concentrations. N=6 *CFTR*$^{+/+}$and 7 *CFTR*$^{\Delta F508/\Delta F508}$.

TABLE 1

CFTR$^{\Delta F508/\Delta F508}$ pigs two or more weeks old.

Case	Sex	Genotype	Type of Surgery	Age	Reason for Euthanasia
1	M	*ΔF508/ΔF508*	loop ileostomy	13 d	prolapsed ostomy
2	F	*ΔF508/ΔF508*	cecostomy	62 d	gastric ulcer*
3	F	*ΔF508/ΔF508*	cecostomy	77 d	poor oral intake, weight loss **
4	F	*ΔF508/ΔF508*	cecostomy	87 d	prolapsed ostomy

* Gastric ulcer has previously been reported to occur in both non-CF and CF pigs (25).

** Etiology of poor oral intake and weight loss was not identified. Pig was hypothermic prior to euthanasia and on post-mortem examination the stomach and proximal small intestine had a large quantity of luminal material suggestive of an ileus. Clinically, the animal appeared septic, but bacterial cultures were negative.

TABLE 2

Microbiology of *CFTR*$^{\Delta F508/\Delta 508}$ lung.

		Lung bacteria		
	Case #	**(avg CFU/g)**	**(range)**	**Cultured species**
ΔF508/ΔF508	1	-	-	*
	2	10	10**	Coagulase-negative *Staphylococcus spp.*
	3	115	0–230	*Acinetobacter lwoffii*, *Escherichia coli*, *Leclercia adecarboxylata*
	4	743	230–1650	Alpha-hemolytic *Streptococcus spp.* (3 morphologies), coagulase-negative *Staphylococcus spp.* (3 morph), *E. coli* (2 morphologies), *Enterococcus* spp., *Haemophilus spp.*, *Pasteurella aerogenes*, *Salmonella spp.*
+/+	1	10	10	Alpha-hemolytic *Streptococcus spp.*, *Diphtheroids*
	2	0	0	
	3	0	0	
	4	0	0	

* samples were not collected for microbiology culture.

** n = 1

Table 3

Changes in current and conductance in *CFTR*$^{\Delta F508/\Delta F508}$ epithelia as a percentage of changes in *CFTR*$^{+/+}$ epithelia. Data are changes in Isc in response to forskolin and IBMX and GlyH-101 (ΔIsc_{cAMP}, ΔIsc_{GlyH}), the corresponding changes in Gt (ΔGt_{cAMP}, ΔGt_{GlyH}), changes in apical current induced by adding basolateral nystatin and apical forskolin and IBMX ($\Delta I_{Nyst+cAMP}$) in the presence of a Cl^- concentration gradient, and changes induced by the subsequent addition of GlyH-101 (ΔI_{GlyH}). To correct for any changes in the absence of CFTR, we subtracted values obtained in *CFTR*$^{-/-}$ epithelia, and data were calculated from mean values of individual measurements as (*CFTR*$^{\Delta F508/\Delta F508}$ – *CFTR*$^{-/-}$)/(*CFTR*$^{+/+}$ – *CFTR* $^{-/-}$).

	***CFTR*$^{\Delta F508/\Delta F508}$ (% *CFTR*$^{+/+}$)**			
	Excised nasal	**Excised tracheal**	**Cultured nasal**	**Cultured tracheal**
ΔIsc_{cAMP}	13.7	9.1	15.1	12.4
ΔGt_{cAMP}			15.7	5.6
ΔIsc_{GlyH}	3.2	9.1	31.6	16.5
ΔGt_{GlyH}			13.1	4.2
$\Delta I_{Nyst+cAMP}$			7.7	7.0
ΔI_{GlyH}			8.3	2.0